

Prediction of ternary alkaline-earth metal Sn(II) and Pb(II) chalcogenide semiconductors

Yuwei Li,^{1,2} Li Wang,¹ Yuancun Qiao,¹ Yanbiao Gan,¹ and David J. Singh^{1,2,3,*}

¹North China Institute of Aerospace Engineering, No. 133 Aimin East Road, Langfang, Hebei 065000, China

²Department of Physics and Astronomy, University of Missouri, Columbia, Missouri 65211, USA

³Department of Chemistry, University of Missouri, Columbia, Missouri 65211, USA



(Received 7 March 2020; accepted 11 May 2020; published 26 May 2020)

Sn(II) and Pb(II) compounds, especially chalcogenides, are important functional materials. The complementary properties of these two families of compounds, with differences related to the differences in stability of the divalent state and relativistic effects on the band structures, provide tunability of properties and also can guide searches for new phases. In particular, it suggests the existence of previously unknown ternary Sn(II) and Pb(II) chalcogenide phases. Here, we predict the existence of stable compounds via first-principles global optimization structure searches on the alkaline-earth metal Sn(II) and Pb(II) chalcogenide systems. This leads to five new stoichiometries. These unreported phases, SrSnS₂, SrSnSe₂, SrPbSe₂, BaSnSe₂, and BaPbS₂, are thermodynamically preferred by Sn-rich (or Pb-rich) conditions, which favor the divalent state. They are semiconducting with band gaps ranging from 0.80 to 1.85 eV, strong visible light absorption and relatively light hole and electron effective masses ($<1 m_0$). The valence band maxima of these compounds have antibonding character involving metal *s* and chalcogen *p* character. This is a feature that is often associated with defect tolerant behavior. In addition the compounds show complex band structures of a type that is favorable for thermoelectric performance.

DOI: [10.1103/PhysRevMaterials.4.055004](https://doi.org/10.1103/PhysRevMaterials.4.055004)

I. INTRODUCTION

The main group IV elements, Sn and Pb, have similar electronic configuration, ns^2np^2 , and related physicochemical properties. There are two common valence states in their oxides and chalcogenides, II and IV. There are many stable Sn(II) and Pb(II) oxides and chalcogenides, with diverse functional properties [1–4]. Recently, Sn(II) and Pb(II) compounds have attracted more attention as electronic materials. For example, the high efficiency of lead halide perovskite (CH₃NH₃PbX₃, X = Cl, Br, I)-based photovoltaic devices and the rapid advances in this area has led to renewed interest in the chemistry of these compounds [5–12]. Tin oxide (SnO_x) thin films are the basis of high performance transparent conductors [13]. Pb(II) and Sn(II) chalcogenides are among the highest performance thermoelectric materials [14]. Pb(Zr,Ti)O₃ is an very important ferroelectric and piezoelectric system, and certain complex chalcogenides including Sn₂P₂S₆ and Sn₂P₂Se₆ are known ferroelectric semiconductors [15,16].

There are various chemical factors that lead to the performance of these materials. One is the antibonding hybridization between Sn-5*s* (or Pb-6*s*) and anion *p* states, which can be important in the upper valence bands (VBs). This antibonding character in VBs increases dispersion, and favors hole mobility, similar to the case of the antibonding *p-d* hybridization in monovalent Cu compounds [17,18]. The metal *s* ligand *p* coupling in Sn(II) and Pb(II) compounds can be strong [10,11,13], since these *s* orbitals are rather

spatially delocalized and so the antibonding *s-p* coupling scenario can lead to more dispersive VBs as well as defect tolerance [19–21]. This chemistry can be effective in band-structure engineering, for example in seeking *p*-type transparent conductors [22–26]. Another is the lone pair physics, which additionally involves hybridization between the unoccupied Sn and Pb *p* states and the chalcogen *p* states. This underlies ferroelectricity and piezoelectricity in these compounds [27], may improve the semiconducting properties, e.g., through dielectric screening [28,29], and can strongly affect the lattice thermal conductivity [30]. Furthermore, the *p* orbital character of the band structures of these compounds favors complex band shapes that can be of importance for thermoelectrics [31–33].

The above additionally suggests considerable tunability of properties. This is because these factors depend strongly on the relative energies of the Sn/Pb *s* and *p* levels in relation to the chalcogen *p* levels. In addition it is important to note that the *s* level in the Pb(II) compounds is generally deeper than in the Sn(II) phases relative to the *p* states due to relativistic contraction of the *s* states. This affects band gaps, lone pair activity, and chemical stability. Motivated in part by this, several ternary Sn(II) and Pb(II) compounds, which exhibit interesting and potentially useful physical properties, have been predicted as functional materials based on first principles calculations and other theoretical approaches. These include oxides (Na₂Sn₂O₃ and K₂Sn₂O₃) [22,34,35], sulfides (BaSnS₂, BaSn₂S₃, SrPbS₂, SrPb₃S₄, and Sr₃PbS₄) [36–38], and at least in narrow chemical potential windows, Sr/BaSn₂O₃, Ca/Sr/BaPb₂O₃, and BaPbO₂ [39,40]. An important goal is to find compounds that have both good stability, with sufficiently broad stability windows, and useful properties.

*singhdj@missouri.edu

Here, we report a search for possible phases in the $M_mIV_nVI_{m+n}$ family (with $M = \text{Mg, Ca, Sr and Ba}$, $IV = \text{Sn and Pb}$, $VI = \text{S and Se}$, and $m, n = 1$ and 2). We used first-principles crystal structure prediction methods with unbiased global optimization. The most challenging issue associated with these Sn(II) and Pb(II) ternary chalcogenides is thermodynamic stability relative to the strongly competing tetravalent compounds, the metals, and the stable binary alkaline earth metal oxides and chalcogenides.

We find (1) in the $m:n=1:1$ system, only the large highly electropositive Sr and Ba ions stabilize the ternary chalcogenides, SrSnS_2 , SrSnSe_2 , SrPbSe_2 , BaSnSe_2 , and BaPbS_2 , against decomposition into competing phases in Sn (or Pb) rich conditions, and (2) in the $m:n=1:2$ and $m:n=2:1$ systems, no alkaline-earth metal element stabilizes these with respect to competing phases. The identified previously unknown stable ternary phases are semiconducting. Nevertheless, they show remarkably different electronic properties.

The Sr based chalcogenides have much more dispersive band edges, with much lower hole and electron effective mass (m_h^* and m_e^*) as compared to those of the Ba chalcogenides, especially for m_h^* . This implies better hole and electron mobility for the Sr compounds. The band gaps range from 0.80 to 1.85 eV. It is also noteworthy that the compounds show strong optical absorption above the respective band gaps. This is due to the charge transfer nature of the electronic structures, with hybridized chalcogen p states forming the valence bands and hybridized metal p states making up the conduction bands. We also find that the band structures are complex due to the multiorbital character. This leads to some compounds with high thermoelectric electronic fitness function (EFF) values. The EFF reflects the decoupling between conductivity and thermopower that can arise from nonparabolic bands, for example [41–43].

II. APPROACH

The most stable crystal structures for compositions $M_mIV_nVI_{m+n}$ were searched for based on first principles density functional theory calculations using the crystal structure analysis by particle swarm optimization (CALYPSO) methodology [44,45]. The key feature of this structure search method is its ability to efficiently identify ground-state structures of materials based on only knowledge of chemical composition. This is done by global optimization on the calculated first principles energy landscape. In the present work, we did structure searches up to at least 24 atoms in the unit cell. For each search, population sizes of ≥ 1500 were used to obtain reliable predictions of the structures. It should be noted that while it is impossible in general to exclude the existence of a more complex crystal structure, it can nonetheless be concluded that the finding of a stable phase at a previously unknown composition means that there will be a new phase in the previously unknown composition region. In practice there are many successful predictions of new crystal structures and phases that have been confirmed by experiments based on this approach [44–46].

The first principles density functional theory calculations, including structure relaxations and total energies for the structure prediction, were done with the Perdew-Burke-Ernzerhof

(PBE) generalized gradient approximation (GGA) [47] and the projector-augmented wave (PAW) method [48], as implemented in the VASP code [49]. The $3s^2$ (Mg), $3p^64s^2$ (Ca), $4s^24p^65s^2$ (Sr), $5s^25p^66s^2$ (Ba), $4d^{10}5s^25p^2$ (Sn), $5d^{10}6s^26p^2$ (Pb), $3s^23p^4$ (S), $4s^24p^4$ (Se) states were treated as valence electrons in the PAW pseudopotentials. We used energy cut-offs of 520 eV for the plane-wave expansions and Brillouin zone integration grid spacings of $2\pi \times 0.032 \text{ \AA}^{-1}$. This produced well converged enthalpies. We checked the dynamical stability of the predicted phases by computing the phonon dispersions by the supercell finite difference method implemented in the PHONOPY code [50].

Standard density functionals, such as the PBE-GGA, are designed to produce accurate total energies but do not in general predict reliable electronic structure features, such as band gaps. Therefore, following predictions of new phases, we did band structure, density of states (DOS), and optical calculations using the modified Becke-Johnson (mBJ) potential of Tran and Blaha [51]. This potential gives band gaps in remarkably good accord with experiment for a wide variety of simple semiconductors and insulators [52–54]. For this purpose, we used the general potential linearized augmented plane-wave (LAPW) method [55], as implemented in the WIEN2K code [56]. This is an all electron method.

Spin-orbit coupling (SOC) was included in the electronic structure, optical property, and effective mass calculations. This is important because of the heavy element p states that contribute to the bands in these compounds. The calculations were done using the structures and lattice parameters generated in the structure search. We used LAPW sphere radii of 2.50 Bohr for all atoms in $P2_1/c$, $Pca2_1$ - SrSnSe_2 , $P4/mmm$ - SrPbSe_2 , and $Pca2_1$ - BaPbS_2 , 2.48 Bohr for all atoms in $P4_32_12$ - SrSnSe_2 , 2.42, 2.42, and 2.50 Bohr for Ba, Sn, and Se in $P2_1$ - BaSnSe_2 . The basis set cutoff k_{max} was determined by the criterion $R_{\text{min}}k_{\text{max}} = 9.0$. Here, R_{min} is the smallest of the LAPW sphere radii in the calculation.

The optical properties were obtained for vertical electric dipole transitions using the optical package of the WIEN2K code. We also calculated transport effective masses to gain insight into their potential conductivity if doped. These were calculated as the mass that would give the same transport coefficient, σ/τ as obtained from the actual band structure at 300 K, with the BOLTZTRAP code [57]. This takes into account the effects of nonparabolicity and anisotropy, multiple bands, etc., on carrier transport. EFF values were obtained using the TRANSM code [41], based on transport integrals obtained from BOLTZTRAP [57]. The usefulness of the EFF is that it provides a simple measure that can be applied to semiconductors and that correlates with measures of thermoelectric performance such as the figure of merit, zT , and power factor, but unlike those quantities does not require calculation of relaxation times [41,43].

III. RESULTS AND DISCUSSION

We performed a systematic search for compounds in the $M_mIV_nVI_{m+n}$ family. Of the 48 possible compounds in this family, three stable compounds are reported in literature [37,38], while no experimental reports could be found for the remaining possible compositions. Therefore,

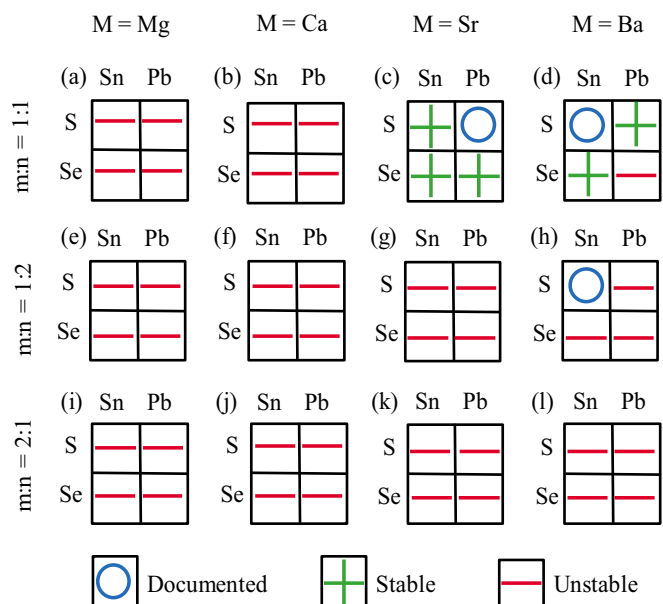


FIG. 1. Summary of calculated thermodynamic stabilities in the $M_mIV_nVI_{m+n}$ family of potential compounds.

crystal structure searches for the missing compounds were conducted and the thermodynamic stability analysis with respect to all of the other competing phases was performed. We predict that five stoichiometries ($P2_1/c$ - $SrSnS_2$, $P4_32_12$ - $SrSnSe_2$, $Pca2_1$ - $SrSnSe_2$, $P4/mmm$ - $SrPbSe_2$, $P2_1$ - $BaSnSe_2$, and $Pca2_1$ - $BaPbS_2$, six compounds in total) out of the missing 45 are stable, as shown in Fig. 1. $P4_32_12$ - $SrSnSe_2$ and $Pca2_1$ - $SrSnSe_2$ are indistinguishable in energy and we list and discuss both of them.

We first discuss thermodynamic stability of the $M_mIV_nVI_{m+n}$ compounds. For this three criteria should be satisfied:

- (1) $m\Delta\mu_M + n\Delta\mu_{IV} + (m+n)\Delta\mu_{VI} = \Delta H_f(M_mIV_nVI_{m+n})$,
- (2) $\Delta\mu_i \leq 0$, ($i = M, IV, VI$), and
- (3) $n_j\Delta\mu_M + m_j\Delta\mu_{IV} + q_j\Delta\mu_{VI} \leq \Delta H_f(M_{n_j}IV_{m_j}VI_{q_j})$, $j = 1, \dots, t$,

where $\Delta\mu_i = \mu_i - \mu_i^0$ is the deviation of actual chemical potential of the atomic species i during growth (μ_i) from that of the bulk elemental solid or gas phase (μ_i^0), ΔH_f is the heat of formation, and $M_{n_j}IV_{m_j}VI_{q_j}$ represents all known j competing phases. These competing phases limit the size of the stable region. Condition (1) is for equilibrium growth, condition (2) is to prevent precipitation to elemental phases of atomic species, and condition (3) is stability against competing phases. Figure 2 shows two-dimensional phase stability diagrams with two independent quantities with $\Delta\mu_M$ and $\Delta\mu_{IV}$ as variables. As seen, there are stable regions only for $SrSnS_2$, $SrSnSe_2$, $SrPbSe_2$, $BaSnSe_2$, and $BaPbS_2$, especially under Sn (or Pb-rich) conditions, i.e., $\Delta\mu_{Sn}$, or $\Delta\mu_{Pb}$ close to zero. The other compounds do not show stability, as seen in the Supplemental Material, Figs. S1– S3 [58].

In addition to thermodynamic stability, we examined the lattice dynamical stability of the six stable phases identified. This is important because one reason for forming a more complex structure with unit cell size larger than that considered in the structure search would be from a phonon instability. However, we do not find any such instabilities. Figure 3 shows the phonon dispersion curves. The labeling of points in the Brillouin zone is given in the Supplemental Material

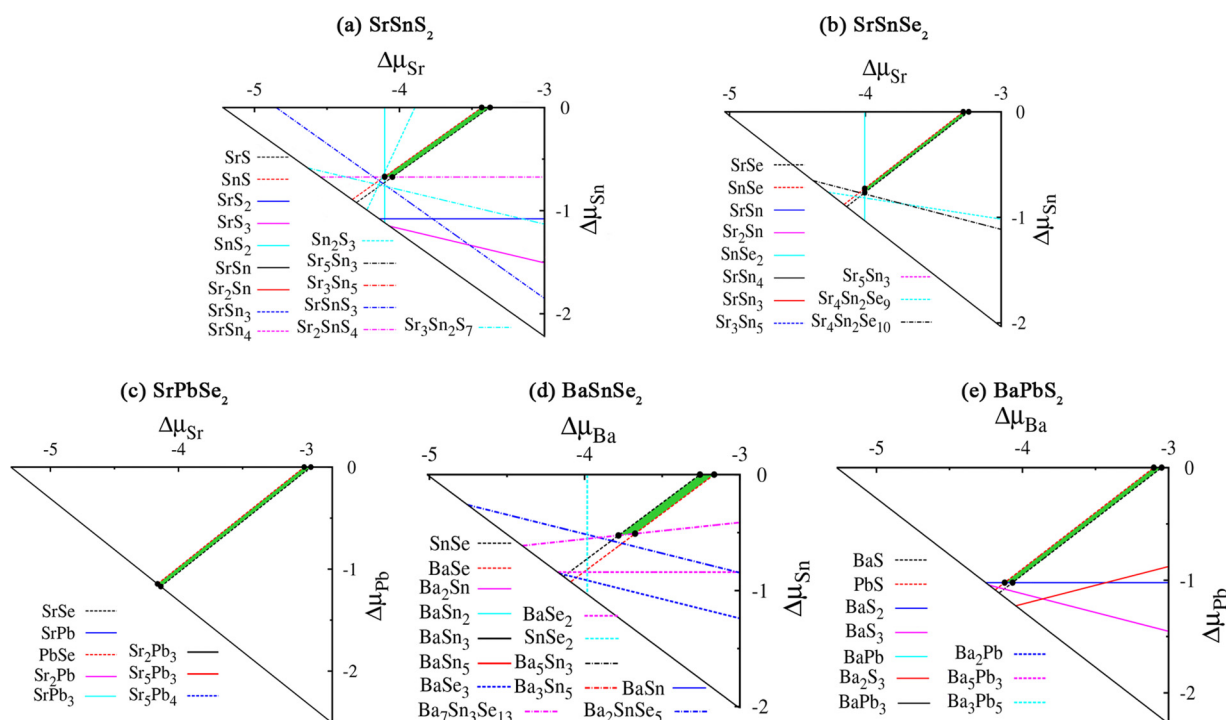


FIG. 2. Phase stability diagrams for (a) $SrSnS_2$, (b) $SrSnSe_2$, (c) $SrPbSe_2$, (d) $BaSnSe_2$, and (e) $BaPbS_2$. Each line represents a known competing phase, and the stable region is indicated in green.

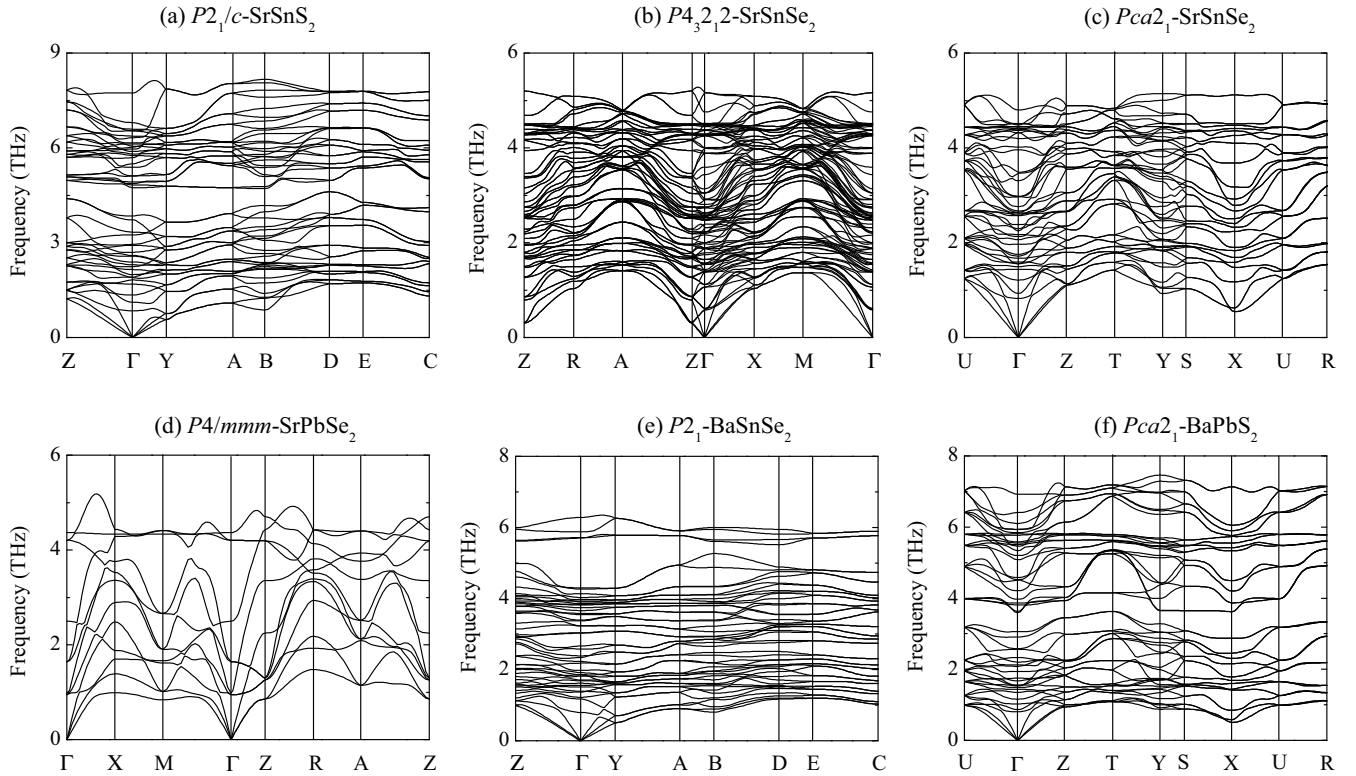


FIG. 3. Calculated phonon dispersions of (a) $P2_1/c$ -SrSnS₂, (b) $P4_32_12$ -SrSnSe₂, (c) $Pca2_1$ -SrSnSe₂, (d) $P4/mmm$ -SrPbSe₂, (e) $P2_1$ -BaSnSe₂, and (f) $Pca2_1$ -BaPbS₂.

(Fig. S4) [58]. The absence of any imaginary phonon modes indicates the dynamical stability of the six structures.

The structures of predicted stable phases, $P2_1/c$ -SrSnS₂, $Pca2_1$ -SrSnSe₂/BaPbS₂, $P4_32_12$ -SrSnSe₂, $P4/mmm$ -SrPbSe₂, and $P2_1$ -BaSnSe₂, are shown in Fig. 4. Detailed structural information is given in Table I. Data for the remaining unstable compounds are given in the Supplemental Material, Tables S1–S3 [58]. The results

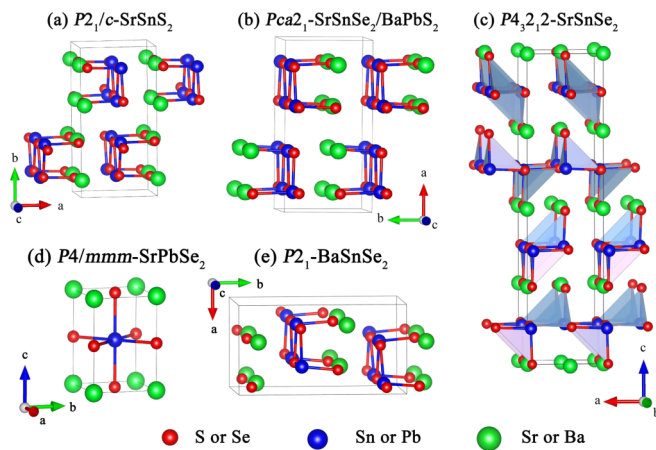


FIG. 4. Lowest-energy structures of (a) $P2_1/c$ -SrSnS₂, (b) $Pca2_1$ -SrSnSe₂/BaPbS₂, (c) $P4_32_12$ -SrSnSe₂, (d) $P4/mmm$ -SrPbSe₂, and (e) $P2_1$ -BaSnSe₂. Red spheres represent S or Se atoms, blue spheres represent Sn or Pb atoms, and bright green spheres represent Sr or Ba atoms.

indicate that by controlling the chemical potentials of the reactants, it should be possible to grow the predicted SrSnS₂, SrSnSe₂, SrPbSe₂, BaSnSe₂, and BaPbS₂ phases. As seen in Fig. 4, $Pca2_1$ -SrSnSe₂ and $Pca2_1$ -BaPbS₂ have the same structural configuration. The structures of $P2_1/c$ -SrSnS₂ and $P4/mmm$ -SrPbSe₂ are similar to the known phases, BaSnS₂ [36] and SrPbS₂ [38], respectively. All the predicted phases, except $P4/mmm$ -SrPbSe₂, are catenate, with basic motif, (IV)(VI)₃, for example, SnS₃ and SnSe₃, polyhedra in which Sn (or Pb) is threefold coordinated by S (or Se). In $P4/mmm$ -SrPbSe₂, there are PbSe₆ octahedra with edge sharing to form three-dimensional structures. The different kinds of (IV)–(VI) coordination and electronic properties (see below) can be rationalized to some extent in terms of chemical differences among the elements. Specifically, Se has a lower electronegativity than S, leading to higher Se p bands, and smaller band gap relative to the corresponding S compound, while the s - p splitting in Pb is larger than in Sn due to relativistic contraction of the s orbital. This stabilizes the Pb(II) valence state.

We now turn to the electronic structures. Figure 5 shows calculated band gaps and hole (electron) transport effective masses. The average effective masses are calculated as the direction average relevant for conductivity, $1/m = (1/m_x + 1/m_y + 1/m_z)/3$. The six predicted compounds show direct or quasidirect band gaps, along with the larger direct gaps being approximately 2 eV. The direct gaps of the stable compounds, $P2_1/c$ -SrSnS₂, $P4_32_12$ -SrSnSe₂, $Pca2_1$ -SrSnSe₂, $P4/mmm$ -SrPbSe₂, $P2_1$ -BaSnSe₂, and $Pca2_1$ -BaPbS₂, are 1.47, 0.93, 0.83,

TABLE I. Structural data for the predicted lowest energy phases, $P2_1/c$ -SrSnS₂, $P4_32_12$ -SrSnSe₂, $Pca2_1$ -SrSnSe₂, $P4/mmm$ -SrPbSe₂, $P2_1$ -BaSnSe₂, and $Pca2_1$ -BaPbS₂, as identified from the structure searches.

Space group	Lattice parameters (Å)	Wyckoff positions	Atoms	x	y	z
SrSnS ₂ $P2_1/c$	$a = 5.9794$	4e	Sr	0.0200	0.8745	0.7610
	$b = 11.9520$		Sn	0.5048	0.8708	0.2764
	$c = 6.0049$	4e	S1	0.5210	0.8508	0.8339
	$\beta = 92.9780^\circ$		S2	0.0604	0.6237	0.7624
SrSnSe ₂ $P4_32_12$	$a = 6.2280$	4a	Sr1	0.9978	0.9978	0.5000
		4a	Sr2	0.4968	0.4968	0.5000
	$c = 24.9337$	8b	Sn	0.5201	0.9891	0.8793
		8b	Se1	0.9740	0.0224	0.6249
SrSnSe ₂ $Pca2_1$	$a = 12.4777$	4a	Sr	0.8750	0.5046	0.9155
			Sn	0.6356	0.9860	0.9314
	$b = 6.2362$	4a	Se1	0.8633	0.0022	0.8943
			Se2	0.8746	0.5296	0.4169
SrPbSe ₂ $P4/mmm$	$a = 4.4135$	1a	Sr	0.0000	0.0000	0.0000
		1d	Pb	0.5000	0.50000	0.5000
	$c = 6.2432$	1c	Se1	0.5000	0.50000	0.0000
		1b	Se2	0.0000	0.0000	0.5000
BaSnSe ₂ $P2_1$	$a = 6.5180$	2a	Ba1	0.8543	0.0944	0.1354
			Ba2	0.3519	0.0792	0.6344
	$b = 12.2611$	2a	Sn1	0.6088	0.3258	0.8328
			Sn2	0.8177	0.8238	0.6706
	$c = 6.4738$	2a	Se1	0.6436	0.5396	0.8633
			Se2	0.8204	0.8160	0.1028
			Se3	0.3981	0.8082	0.6052
			Se4	0.8516	0.0386	0.6378
$\beta = 86.3947^\circ$	2a	Se1	0.8204	0.8160	0.1028	
		Se2	0.3981	0.8082	0.6052	
BaPbS ₂ $Pca2_1$	$a = 12.6460$	4a	Ba	0.8750	0.5046	0.9193
			Pb	0.6368	0.9837	0.9348
	$b = 6.2816$	4a	S1	0.8573	0.0025	0.8831
			S2	0.8748	0.5395	0.4209
$c = 6.3074$	4a	S2	0.8748	0.5395	0.4209	

0.80, 1.65, and 1.86 eV, respectively. The four Sr-based compounds have lower band gaps than the Ba-based phases. The four Sr-based chalcogenides have both low m_h^* and m_e^* . The two Ba-based compounds have moderate m_h^* and m_e^* . This may reflect the larger size of the Ba cations, which then favors longer bond distances and weaker dispersion. The averaged m_h^* (m_e^*) are 0.31 (0.39), 0.24 (0.50), 0.21 (0.25), 0.20 (0.17), 0.90 (0.82), 0.58 (0.39) m_0 for $P2_1/c$ -SrSnS₂, $P4_32_12$ -SrSnSe₂, $Pca2_1$ -SrSnSe₂, $P4/mmm$ -SrPbSe₂, $P2_1$ -BaSnSe₂, and $Pca2_1$ -BaPbS₂, respectively.

The effective masses are consistent with the trend in the band gaps. Specifically, the lower band gap compounds have lower m_h^* , which would be the expected trend for a case in which band dispersion is the main factor that closes a gap between ionic levels. This is a reasonable starting point for these compounds, which as mentioned have band gaps of charge transfer character. The m^* , especially the m_h^* , of $P4_32_12$ -SrSnSe₂, $Pca2_1$ -SrSnSe₂, $P4/mmm$ -SrPbSe₂ are significantly lower than for the other compounds. There is also an anisotropy of the m^* , as seen in Fig. 5(b). This is an expected consequence of the layered structures. The absorption spectra and transport properties (σ/τ) are shown in

Fig. 6 and Supplemental Material, Fig. S5 [58]. The transport properties show reasonably high reduced conductivity σ/τ for several of the compounds, as compared with standard thermoelectrics such as PbTe and rhombohedral GeTe. This is the case for both p -type and n -type. Comparison with experiment will be useful in characterizing the electronic structure should the compounds be synthesized. As seen, the compounds show strong absorption in visible light range. Considering the moderate values of the effective masses, the compounds may show significant photoelectric response with ambipolar conductivity in the context of photovoltaics.

Figures 7 and 8 show the band structures and corresponding projected densities of states (DOS) for the six compounds. As mentioned, the band gaps of these ternary compounds are widened relative to the binary Sn(II) [or Pb(II)] chalcogenides, 1.30 eV for SnS [59,60], ~ 0.86 eV for SnSe [61], 0.41 eV for PbS [62], and 0.26 eV for PbSe [63]. Similar trends have been found in oxides with s - p and p - d hybridization dominating VB maxima, e.g., from SnO [64,65] to Sr/BaSn₂O₃ [39] and from PbO [66] to Ca/Sr/BaPb₂O₃ [40] and from Cu₂O [67] to CuAlO₂ [17].

The valence bands are primarily from chalcogen p states. These hybridize with s and p states of the group IV atom.

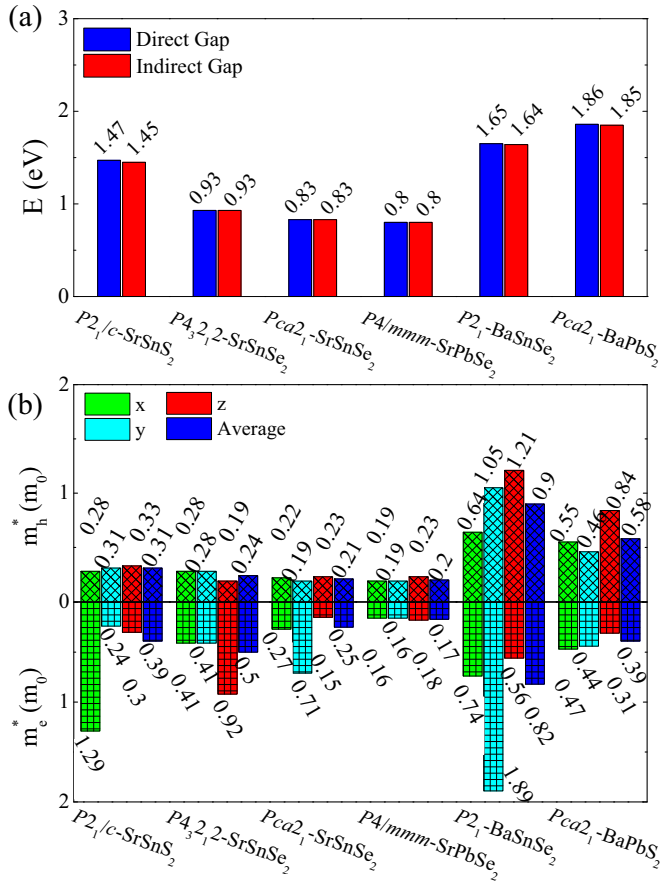


FIG. 5. (a) Calculated direct/indirect band gaps and (b) direction dependent (x , y , and z) and average effective masses of m_h^* and m_e^* for $P2_1/c$ -SrSnS₂, $P4_32_12$ -SrSnSe₂, $Pca2_1$ -SrSnSe₂, $P4/mmm$ -SrPbSe₂, $P2_1$ -BaSnSe₂, and $Pca2_1$ -BaPbS₂.

The conduction bands come from group IV- p orbitals, again hybridized with chalcogen p states. As usual, antibonding character is important for the states at the top of the valence bands. This involves hybridization with the Sn- s or Pb- s orbital. The antibonding character is unambiguously indicated by the crystal orbital overlap population (COOP) [68].

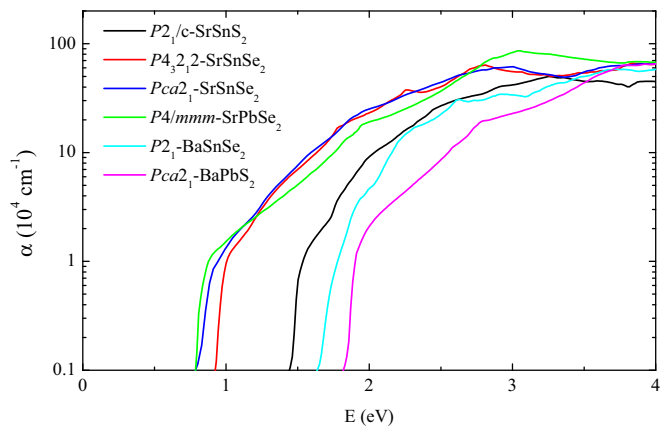


FIG. 6. Absorption spectra for $P2_1/c$ -SrSnS₂ (black), $P4_32_12$ -SrSnSe₂ (red), $Pca2_1$ -SrSnSe₂ (blue), $P4/mmm$ -SrPbSe₂ (bright green), $P2_1$ -BaSnSe₂ (cyan), and $Pca2_1$ -BaPbS₂ (magenta).

These are shown in Supplemental Material, Fig. S6 [58], with positive $n(e)$ representing bonding and negative $n(e)$ representing antibonding. In addition to the Sn(or Pb)- s states, there are substantial Sn(or Pb)- p states in VBs, forming bonding states with S(or Se)- p orbitals. This hybridization is then important for the values of the hole effective mass, m_h^* . Large IV-VI-IV bond angles maximize the overlap for this hopping channel, providing dispersion and reduction of the m_h^* [69]. Specifically, IV-VI-IV bond angles near 180° maximize the overlap and minimize the hole effective mass. This is consistent with our result that the $P4/mmm$ -SrPbSe₂ phase has the lowest m_h^* and the maximal IV-VI-IV bond angle of 180° .

It is also interesting to note that BaPbS₂, $Pca2_1$ -SrSnSe₂, and BaSnSe₂ show shifts of the conduction band minima away from high symmetry points. This is as expected from the Rashba effect in these noncentrosymmetric structures. Such a splitting is also seen in $P4_32_12$ -SrSnSe₂ for the conduction band pocket at the A point.

Thermoelectric performance is characterized by a figure of merit, $zT = \sigma S^2 T / \kappa$, which is a combination of electrical and thermal transport quantities. Here σ is electrical conductivity, S is thermopower, T is temperature, and κ is thermal conductivity. High zT is a counterindicated property, meaning that it requires a combination of transport properties that are not usually found, especially the combination of high σ and high S [14,70–72]. High σ generally requires light mass bands, as this leads to high mobility. On the other hand, high S requires strong energy dependence and is generally associated with heavy mass. This conundrum can be resolved by band structures that behave differently for σ and S , and it is this different behavior that the EFF quantifies [43]. As an example, calculations of the EFF previously led to the prediction that cubic p -type GeTe would be an excellent thermoelectric in the temperature range where the material is normally rhombohedral [33]. This prediction was supported by experiments that showed that indeed stabilized cubic p -type GeTe is a very high performance thermoelectric [73,74]. Binary PbSe [75,76], PbS [77,78], PbTe [79–81], and SnTe [82–84] are known thermoelectric materials with high zT (and EFF) values. We note that the relatively low-frequency phonons and the heavy Sn (or Pb) atoms may lead to low thermal conductivity. The compounds identified here show complex band structures near the band extrema, including multiple bands, multiple carrier pockets, and nonparabolic shapes. The combination of likely low thermal conductivity and complex bands may be favorable for thermoelectric performance. As such, if synthesized, it will be of interest to investigate these compounds as thermoelectrics. We calculated the direction dependent EFF, which is a measure of the extent to which a band structure has features that decouple the thermopower from the conductivity. This is one indicator of thermoelectric performance. These EFF are plotted as a function of carrier concentration for the best (highest EFF) direction in Fig. 9 [41]. For comparison the state of the art thermoelectric materials, p -type PbTe, n -type PbSe, and n -type ZrNiSn have maximum EFF values at the temperature with highest zT of 2.4×10^{-19} , 1.6×10^{-19} , and 1.0×10^{-19} , respectively, in the same units [41].

We find that $P2_1/c$ -SrSnS₂ and $Pca2_1$ -SrSnSe₂ may have good thermoelectric properties at 800 K for n -type (with

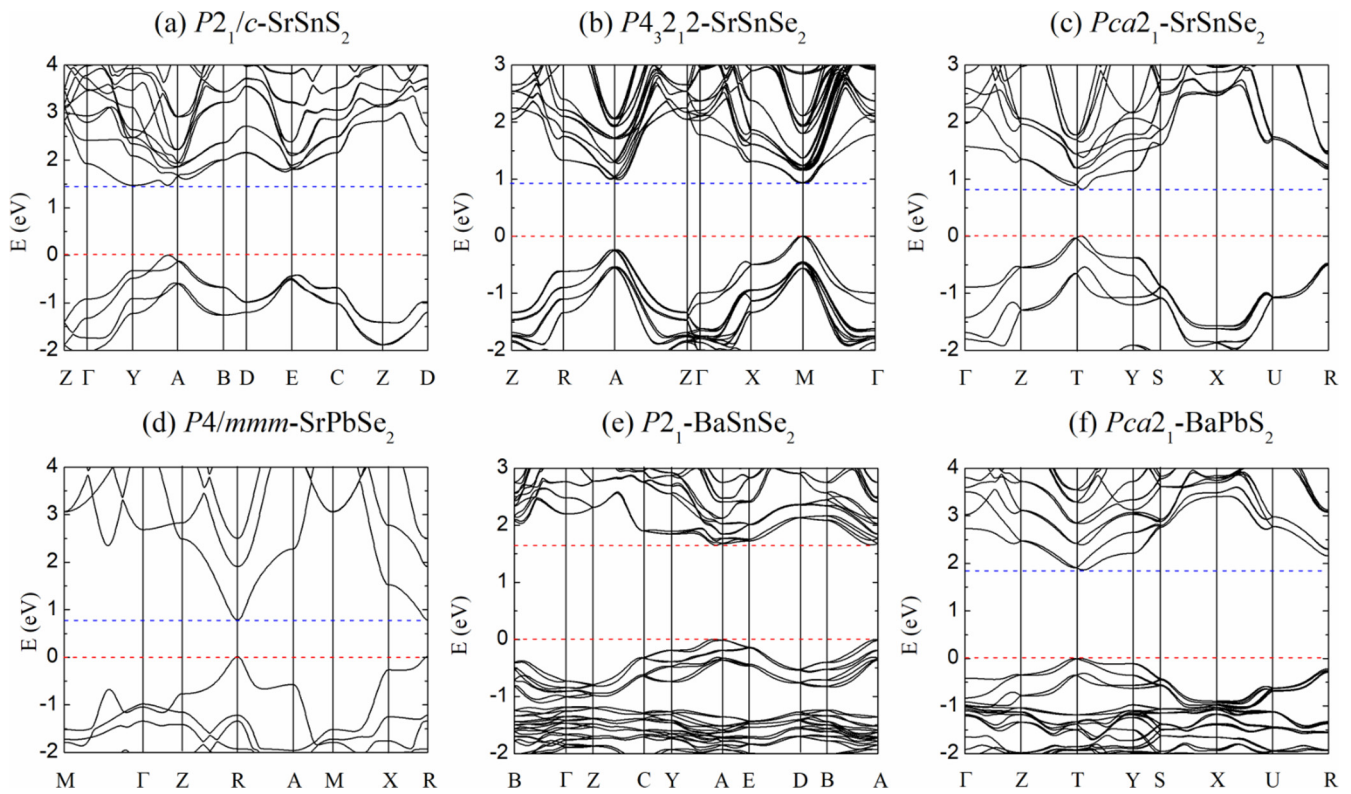


FIG. 7. Calculated band structures of (a) $P2_1/c$ -SrSnS₂, (b) $P4_32_12$ -SrSnSe₂, (c) $Pca2_1$ -SrSnSe₂, (d) $P4/mmm$ -SrPbSe₂, (e) $P2_1$ -BaSnSe₂, and (f) $Pca2_1$ -BaPbS₂.

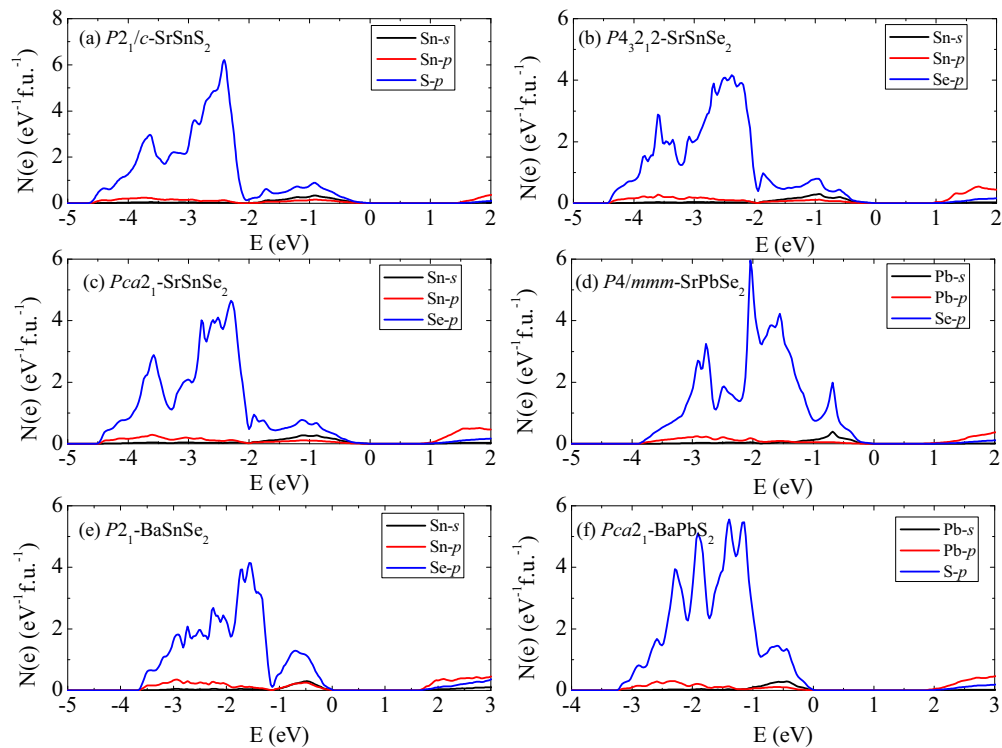


FIG. 8. Projected electronic density of states of (a) $P2_1/c$ -SrSnS₂, (b) $P4_32_12$ -SrSnSe₂, (c) $Pca2_1$ -SrSnSe₂, (d) $P4/mmm$ -SrPbSe₂, (e) $P2_1$ -BaSnSe₂, and (f) $Pca2_1$ -BaPbS₂ of Sn-s or Pb-s (black), Sn-p or Pb-p (red), and S-p or Se-p (blue) character. The energy zero is at the valence band maximum.

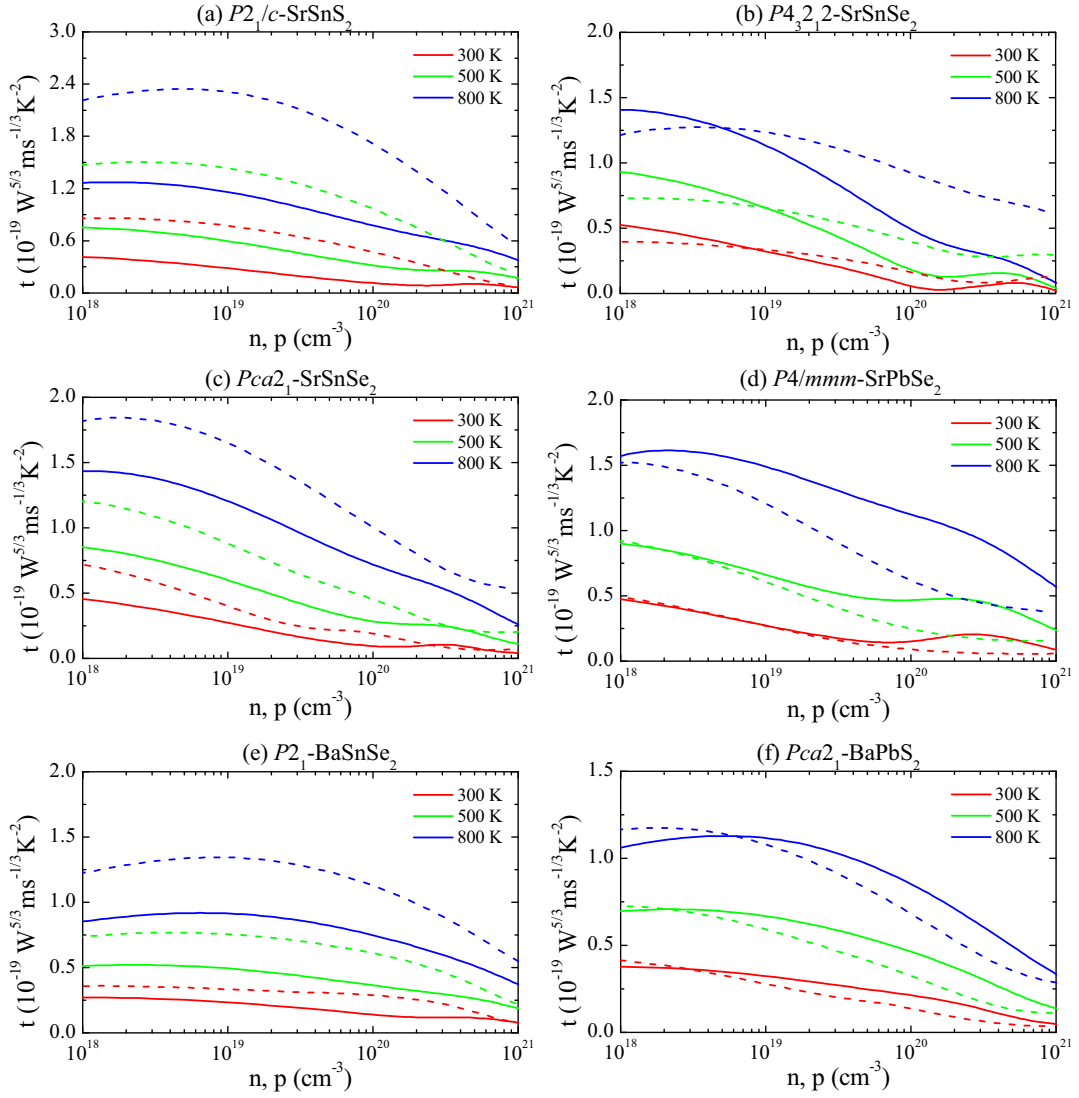


FIG. 9. Calculated best direction component of the anisotropic electronic fitness function (EFF) at 300, 500, and 800 K with respect to the carrier concentration for p -type (solid lines) and n -type (dashed lines). (a) $P2_1/c$ -SrSnS₂, (b) $P4_3_2_1_2$ -SrSnSe₂, (c) $Pca2_1$ -SrSnSe₂, (d) $P4/mmm$ -SrPbSe₂, (e) $P2_1$ -BaSnSe₂, and (f) $Pca2_1$ -BaPbS₂.

carrier concentration $\sim 5 \times 10^{18}$ and $2 \times 10^{18} \text{ cm}^{-3}$), according to the EFF. It should be noted that spin orbit coupling plays an important role in the band structures of these compound as shown in supplemental Fig. S7 for SrPbSe₂. This is especially the case for the conduction bands relevant to n -type, which is as may be expected since the conduction bands in this compound have sizable Pb p character. It is important also to note the nonparabolic band shape at the band edges in this compound and in particular that the band becomes noticeably heavier as one moves away from the band edge. This is a consequence of spin orbit and is seen in the conduction band by the downward curvature of the lowest conduction band at R . Such nonparabolic features are important for the EFF. As seen, both of these compounds have Seebeck coefficients (see Supplemental Material, Fig. S8) [58], $250 \mu\text{V/K} < |S| < 500 \mu\text{V/K}$, for doping levels near the EFF maximum. This is in the range of values for known high performance thermoelectrics. Importantly, these

compounds, which show high EFF also show the combination of high S and high σ/τ (see Supplemental Material, Figs. S4 and S7) [58], which would lead to a high reduced power factor, $\sigma S^2/\tau$.

IV. SUMMARY AND CONCLUSIONS

We report the prediction of six stable alkaline earth Sn(II) or Pb(II) ternary chalcogenides, $M_mIV_nVI_{m+n}$ (with $M = \text{Mg, Ca, Sr and Ba}$, $IV = \text{Sn and Pb}$, and $VI = \text{S and Se}$), based on crystal structure prediction methods. These are $P2_1/c$ -SrSnS₂, $P4_3_2_1_2$ -SrSnSe₂, $Pca2_1$ -SrSnSe₂, $P4/mmm$ -SrPbSe₂, $P2_1$ -BaSnSe₂, and $Pca2_1$ -BaPbS₂. They show both lattice dynamical stability and thermodynamic stability with respect to competing phases. The $M_mIV_nVI_{m+n}$ family containing alkaline/alkaline-earth metals follows Zintl behavior in that the alkaline-earth metal ions serve to supply electrons to the IV-VI framework, occupy space, and

stabilize the structures. They all show band gaps consistent with semiconducting behavior, with a range between 0.8 eV and 1.85 eV. The band gaps are of charge transfer character between mainly chalcogen p derived valence bands and mainly Sn or Pb p derived conduction band states. This leads to strong visible light absorption. These compounds additionally have low to modest transport effective masses, especially for the Sr compounds. This reflects the bonding of the compounds, which includes significant antibonding hybridization between Sn s or Pb s and chalcogen p orbitals at the valence band maximum. Additionally, the p derived band edges lead to complex nonparabolic band structures, which combined with the lone-pair crystal chemistry may lead to interesting thermo-

electric behavior. It will be of interest to verify these phases by experimental synthesis and, if successful, to experimentally measure the electronic and optical properties and to perform doping studies.

ACKNOWLEDGMENTS

Y.L. acknowledges funding support from National Natural Science Foundation of China under Grant No. 11904010. Y.Q. acknowledges funding support from Natural Science Foundation of Hebei Province under Grant No. A2019409043. Y.G. acknowledges funding support from National Natural Science Foundation of China under Grant No. 11875001.

-
- [1] N. N. Greenwood and A. Earnshaw, *Chemistry of the Elements* (Elsevier, Amsterdam, 2012).
- [2] J. Leciejewicz, *Acta Crystallogr.* **14**, 1304 (1961).
- [3] R. J. Hill, *Acta Crystallogr., Sect. C: Cryst. Struct. Commun.* **41**, 1281 (1985).
- [4] J. Pannetier and G. Denes, *Acta Crystallogr., Sect. B: Struct. Crystallogr. Cryst. Chem.* **36**, 2763 (1980).
- [5] A. Kojima, K. Teshima, Y. Shirai, and T. Miyasaka, *J. Am. Chem. Soc.* **131**, 6050 (2009).
- [6] B. V. Lotsch, *Angew. Chem. Int. Ed.* **53**, 635 (2014).
- [7] N.-G. Park, *J. Phys. Chem. Lett.* **4**, 2423 (2013).
- [8] H. J. Snaith, *J. Phys. Chem. Lett.* **4**, 3623 (2013).
- [9] H. Zhou, Q. Chen, G. Li, S. Luo, T.-b. Song, H.-S. Duan, Z. Hong, J. You, Y. Liu, and Y. Yang, *Science* **345**, 542 (2014).
- [10] W. Nie, H. Tsai, R. Asadpour, J.-C. Blancon, A. J. Neukirch, G. Gupta, J. J. Crochet, M. Chhowalla, S. Tretiak, M. A. Alam *et al.*, *Science* **347**, 522 (2015).
- [11] A. Mei, X. Li, L. Liu, Z. Ku, T. Liu, Y. Rong, M. Xu, M. Hu, J. Chen, Y. Yang *et al.*, *Science* **345**, 295 (2014).
- [12] F. Hao, C. C. Stoumpos, D. H. Cao, R. P. H. Chang, and M. G. Kanatzidis, *Nat. Photonics* **8**, 489 (2014).
- [13] A. Behrendt, C. Friedenberger, T. Gahlmann, S. Trost, T. Becker, K. Zilberberg, A. Polywka, P. Görrn, and T. Riedl, *Adv. Mater.* **27**, 5961 (2015).
- [14] C. Wood, *Rep. Prog. Phys.* **51**, 459 (1988).
- [15] R. V. Gamernyk, Y. P. Gnatenko, P. M. Bukivskij, P. A. Skubenko, and V. Y. Slivka, *J. Phys.: Condens. Matter* **18**, 5323 (2006).
- [16] I. V. Kityk, R. I. Mervinskii, J. Kasperczyk, and S. Jossi, *Mater. Lett.* **27**, 233 (1996).
- [17] H. Kawazoe, M. Yasukawa, H. Hyodo, M. Kurita, H. Yanagi, and H. Hosono, *Nature (London)* **389**, 939 (1997).
- [18] S.-i. Inoue, K. Ueda, H. Hosono, and N. Hamada, *Phys. Rev. B* **64**, 245211 (2001).
- [19] A. Walsh and A. Zunger, *Nat. Mater.* **16**, 964 (2017).
- [20] W. Meng, B. Saparov, F. Hong, J. Wang, D. B. Mitzi, and Y. Yan, *Chem. Mater.* **28**, 821 (2016).
- [21] J. Kang and L. W. Wang, *J. Phys. Chem. Lett.* **8**, 489 (2017).
- [22] G. Hautier, A. Miglio, G. Ceder, G.-M. Rignanese, and X. Gonze, *Nat. Commun.* **4**, 2292 (2013).
- [23] A. Walsh and G. W. Watson, *Phys. Rev. B* **70**, 235114 (2004).
- [24] G. W. Watson, S. C. Parker, and G. Kresse, *Phys. Rev. B* **59**, 8481 (1999).
- [25] S. B. Zhang, S.-H. Wei, A. Zunger, and H. Katayama-Yoshida, *Phys. Rev. B* **57**, 9642 (1998).
- [26] R. E. Brandt, V. Stevanović, D. S. Ginley, and T. Buonassisi, *MRS Commun.* **5**, 265 (2015).
- [27] R. E. Cohen, *Nature (London)* **358**, 136 (1992).
- [28] M. H. Du, *J. Mater. Chem. A* **2**, 9091 (2014).
- [29] X. He, D. J. Singh, P. Boon-on, M. W. Lee, and L. Zhang, *J. Am. Chem. Soc.* **140**, 18058 (2018).
- [30] M. D. Nielsen, V. Ozolins, and J. P. Heremans, *Energy Environ. Sci.* **6**, 570 (2013).
- [31] D. J. Singh, *Phys. Rev. B* **81**, 195217 (2010).
- [32] G. Tan, L. D. Zhao, and M. G. Kanatzidis, *Chem. Rev.* **116**, 12123 (2016).
- [33] G. Xing, J. Sun, X. Fan, W. Zheng, and D. J. Singh, *J. Appl. Phys.* **123**, 195105 (2018).
- [34] R. M. Braun and R. Hoppe, *Angew. Chem., Int. Ed. Engl.* **17**, 449 (1978).
- [35] R. M. Braun and R. Hoppe, *Z. Naturforsch. B* **37**, 688 (1982).
- [36] J. E. Iglesias and H. Steinfink, *Acta Crystallogr., Sect. B: Struct. Crystallogr. Cryst. Chem.* **29**, 1480 (1973).
- [37] S. Del Bucchia, J. C. Jumas, and M. Maurin, *Acta Crystallogr., Sect. B: Struct. Crystallogr. Cryst. Chem.* **36**, 2935 (1980).
- [38] S. Hao, L.-D. Zhao, C.-Q. Chen, V. P. Dravid, M. G. Kanatzidis, and C. M. Wolverton, *J. Am. Chem. Soc.* **136**, 1628 (2014).
- [39] Y. Li, D. J. Singh, M.-H. Du, Q. Xu, L. Zhang, W. Zheng, and Y. Ma, *J. Mater. Chem. C* **4**, 4592 (2016).
- [40] Y. Li, L. Zhang, and D. J. Singh, *Phys. Rev. Mater.* **1**, 055001 (2017).
- [41] G. Xing, J. Sun, Y. Li, X. Fan, W. Zheng, and D. J. Singh, *Phys. Rev. Mater.* **1**, 065405 (2017).
- [42] J. Sun and D. J. Singh, *J. Mater. Chem. A* **5**, 8499 (2017).
- [43] Z. Feng, Y. Fu, A. Putatunda, Y. Zhang, and D. J. Singh, *Phys. Rev. B* **100**, 085202 (2019).
- [44] Y. Wang, J. Lv, L. Zhu, and Y. Ma, *Phys. Rev. B* **82**, 094116 (2010).
- [45] Y. Wang, J. Lv, L. Zhu, and Y. Ma, *Comput. Phys. Commun.* **183**, 2063 (2012).
- [46] W. Cui and Y. Li, *Chin. Phys. B* **28**, 107104 (2019).
- [47] J. P. Perdew, K. Burke, and M. Ernzerhof, *Phys. Rev. Lett.* **77**, 3865 (1996).

- [48] G. Kresse and D. Joubert, *Phys. Rev. B* **59**, 1758 (1999).
- [49] G. Kresse and J. Furthmüller, *Phys. Rev. B* **54**, 11169 (1996).
- [50] A. Togo and I. Tanaka, *Scr. Mater.* **108**, 1 (2015).
- [51] F. Tran and P. Blaha, *Phys. Rev. Lett.* **102**, 226401 (2009).
- [52] D. Koller, F. Tran, and P. Blaha, *Phys. Rev. B* **83**, 195134 (2011).
- [53] Y. Li, J. Sun, and D. J. Singh, *Appl. Phys. Lett.* **110**, 051904 (2017).
- [54] Y. Li and D. J. Singh, *Phys. Rev. Mater.* **1**, 075402 (2017).
- [55] D. J. Singh and L. Nordstrom, *Planewaves, Pseudopotentials, and the LAPW method*, 2nd ed. (Springer, Berlin, 2006).
- [56] P. Blaha, K. Schwarz, G. K. H. Madsen, D. Kvasnicka, and J. Luitz, *WIEN2k, An Augmented Plane Wave + Local Orbitals Program for Calculating Crystal Properties* (Technische Universität Wien, Wien, Austria, 2001).
- [57] G. K. H. Madsen and D. J. Singh, *Comput. Phys. Commun.* **175**, 67 (2006).
- [58] See Supplemental Material at <http://link.aps.org/supplemental/10.1103/PhysRevMaterials.4.055004> for information including detailed data on structure and phase stability as well as details of transport properties.
- [59] K. R. Reddy, N. K. Reddy, and R. Miles, *Sol. Energy Mater. Sol. Cells* **90**, 3041 (2006).
- [60] H. Noguchi, A. Setiyadi, H. Tanamura, T. Nagatomo, and O. Omoto, *Sol. Energy Mater. Sol. Cells* **35**, 325 (1994).
- [61] G. Shi and E. Kioupakis, *J. Appl. Phys.* **117**, 065103 (2015).
- [62] Y. Wang, A. Suna, W. Mahler, and R. Kasowski, *J. Chem. Phys.* **87**, 7315 (1987).
- [63] J. M. Pietryga, R. D. Schaller, D. Werder, M. H. Stewart, V. I. Klimov, and J. A. Hollingsworth, *J. Am. Chem. Soc.* **126**, 11752 (2004).
- [64] N. Quackenbush, J. Allen, D. Scanlon, S. Sallis, J. Hewlett, A. Nandur, B. Chen, K. Smith, C. Weiland, D. Fischer *et al.*, *Chem. Mater.* **25**, 3114 (2013).
- [65] Y. Ogo, H. Hiramatsu, K. Nomura, H. Yanagi, T. Kamiya, M. Hirano, and H. Hosono, *Appl. Phys. Lett.* **93**, 032113 (2008).
- [66] R. C. Keezer, D. L. Bowman, and J. H. Becker, *J. Appl. Phys.* **39**, 2062 (1968).
- [67] E. Ruiz, S. Alvarez, P. Alemany, and R. A. Evarestov, *Phys. Rev. B* **56**, 7189 (1997).
- [68] S. Maintz, V. L. Deringer, A. L. Tchougréeff, and R. Dronskowski, *J. Comput. Chem.* **34**, 2557 (2013).
- [69] V.-A. Ha, F. Ricci, G.-M. Rignanese, and G. Hautier, *J. Mater. Chem. C* **5**, 5772 (2017).
- [70] D. M. Rowe, *Thermoelectrics Handbook* (CRC Press, Boca Raton, 2006).
- [71] Z. G. Chen, G. Han, L. Yang, L. Cheng, and J. Zou, *Prog. Nat. Sci.: Mater. Int.* **22**, 535 (2012).
- [72] J. Yang, L. Xi, W. Qiu, L. Wu, X. Shi, L. Chen, J. Yang, W. Zhang, C. Uher, and D. J. Singh, *NPJ Comput. Mater.* **2**, 15015 (2016).
- [73] Z. Liu, J. Sun, J. Mao, H. Zhu, W. Ren, J. Zhou, Z. Wang, D. J. Singh, J. Sui, C. W. Chu, and Z. Ren, *Proc. Nat. Acad. Sci.* **115**, 5332 (2018).
- [74] T. Xing, Q. Song, P. Qiu, Q. Zhang, X. Xia, J. Liao, R. Liu, H. Huang, J. Yang, S. Bai, D. Ren, X. Shi, and L. Chen, *Natl. Sci. Rev.* **6**, 944 (2019).
- [75] L.-D. Zhao, S. Hao, S.-H. Lo, C.-I. Wu, X. Zhou, Y. Lee, H. Li, K. Biswas, T. P. Hogan, C. Uher *et al.*, *J. Am. Chem. Soc.* **135**, 7364 (2013).
- [76] H. Wang, Y. Pei, A. D. LaLonde, and G. J. Snyder, *Proc. Natl. Acad. Sci.* **109**, 9705 (2012).
- [77] H. Wang, E. Schechtel, Y. Pei, and G. J. Snyder, *Adv. Energy Mater.* **3**, 488 (2013).
- [78] L.-D. Zhao, J. He, C.-I. Wu, T. P. Hogan, X. Zhou, C. Uher, V. P. Dravid, and M. G. Kanatzidis, *J. Am. Chem. Soc.* **134**, 7902 (2012).
- [79] Y. Pei, A. LaLonde, S. Iwanaga, and G. J. Snyder, *Energy Environ. Sci.* **4**, 2085 (2011).
- [80] A. D. LaLonde, Y. Pei, and G. J. Snyder, *Energy Environ. Sci.* **4**, 2090 (2011).
- [81] K. Biswas, J. He, I. D. Blum, C.-I. Wu, T. P. Hogan, D. N. Seidman, V. P. Dravid, and M. G. Kanatzidis, *Nature (London)* **489**, 414 (2012).
- [82] G. Tan, F. Shi, S. Hao, H. Chi, L.-D. Zhao, C. Uher, C. Wolverton, V. P. Dravid, and M. G. Kanatzidis, *J. Am. Chem. Soc.* **137**, 5100 (2015).
- [83] A. Banik and K. Biswas, *J. Mater. Chem. A* **2**, 9620 (2014).
- [84] G. Tan, L.-D. Zhao, F. Shi, J. W. Doak, S.-H. Lo, H. Sun, C. Wolverton, V. P. Dravid, C. Uher, and M. G. Kanatzidis, *J. Am. Chem. Soc.* **136**, 7006 (2014).